[Articles in Press](#)[Current Issue](#)

Journal Archive

[+ Volume 32 \(2025\)](#)[+ Volume 31 \(2024\)](#)[+ Volume 30 \(2023\)](#)[+ Volume 29 \(2022\)](#)[+ Volume 28 \(2021\)](#)[+ Volume 27 \(2020\)](#)[+ Volume 26 \(2019\)](#)[+ Volume 25 \(2018\)](#)[+ Volume 24 \(2017\)](#)[+ Volume 23 \(2016\)](#)[- Volume 22 \(2015\)](#)[Issue 6](#)[Transactions on Nanotechnology \(F\)](#)[Issue 6](#)[Transactions on Industrial Engineering \(E\)](#)[Issue 6](#)[Transactions on Computer Science & Engineering and Electrical Engineering \(D\)](#)[Issue 6](#)[Transactions on Chemistry and Chemical Engineering \(C\)](#)[Issue 6](#)[Transactions on Mechanical Engineering \(B\)](#)[Issue 6](#)[Transactions on Civil Engineering \(A\)](#)[Issue 5](#)[Transactions on Mechanical Engineering \(B\)](#)[Issue 5](#)[Transactions on Civil Engineering \(A\)](#)[Issue 4](#)Volume & Issue: Volume 22, Issue 3, Transactions on Civil Engineering (A), May and June 2015 [🔗](#)

Number of Articles: 12

A synopsis about the effect of metakaolin on the durability of Portland cement – An overview

Pages 579-603

Alaa M. Rashad

[View Article](#) [PDF](#) 1.73 M

Nonlinear Behavior of Concrete End Diaphragms in Straight Slab-Girder Bridges

Pages 604-614

Himan Hojat Jalali; Shervin Maleki

[View Article](#) [PDF](#) 5.39 M [Scopus](#) 2

Nonlinear Finite Element Analysis of Rectangular Reinforced Concrete Slabs Strengthened by Fiber Reinforced Plastics

Pages 615-628

Cindrawaty Lesmana; Hsuan-Teh Hu

[View Article](#) [PDF](#) 4.82 M [Scopus](#) 4

Pile head displacements with different cross sectional shapes under lateral loading and unloading in granular soils

Pages 629-638

Pejman Vahabkashi; Alireza Rahai

[View Article](#) [PDF](#) 4.57 M [Scopus](#) 1

Development of Nonlinear Transfer Matrix Method for Inelastic Analyses of Beams

Pages 639-649

Minho Kwon; Minho Kwon; Jinsup Kim; Jinsup Kim; Hyunsu Seo; Suchart Limkatanyu

[View Article](#) [PDF](#) 4.02 M

Bi-Level Optimization of Resource-Constrained Multiple Project Scheduling Problems in Hydropower Station Construction under Uncertainty

Pages 650-667

Zhe Zhang; Jiuping Xu; Hui Yang; Yang Wang

[View Article](#) [PDF](#) 8.09 M [Scopus](#) 5

Integrating system dynamics and fuzzy bargaining for quantitative risk allocation in construction projects

Pages 668-678

Farnad Nasirzadeh; Mehdi Rouhparvar; Hamed Mazandarani Zadeh; Mahdi Rezaie

[View Article](#) [PDF](#) 5.62 M [Scopus](#) 7

Measuring wave velocity, damping and stress-strain behaviors of geo-materials using GAP-SENSOR

Pages 679-698

A. Aghaei Araei; A. Aghaei Araei; I. Towhata; S. Hashemi Tabatabaei; H.R. Razeghi; S. Hashemi Tabatabaei

[View Article](#) [PDF](#) 7.23 M [Scopus](#) 1

Shear-Torsion Interaction of RC Beams Strengthened with FRP Sheets

Pages 699-708












Sayed Behzad Talaeitaba; Davood Mostofinejad

[View Article](#) [PDF](#) 2.98 M [Scopus](#) 5

Extent of riprap layer with different stone sizes around rectangular bridge piers with or without an attached collar

Pages 709-716

M. Karimaei Tabarestani; A. R. Zarrati; M. B. Mashahir; E. Mokallaf

Transactions on Mechanical Engineering (B)
 Issue 4
Transactions on Civil Engineering (A)
 Issue 3
Transactions on Nanotechnology (F)
 Issue 3
Transactions on Industrial Engineering (E)
 Issue 3
Transactions on Computer Science & Engineering and Electrical Engineering (D)
 Issue 3
Transactions on Chemistry and Chemical Engineering (C)
 Issue 3
Transactions on Mechanical Engineering (B)
 Issue 3
Transactions on Civil Engineering (A)
 Issue 2
Transactions on Mechanical Engineering (B)
 Issue 2
Transactions on Civil Engineering (A)
 Issue 1
Transactions on Mechanical Engineering (B)
 Issue 1
Transactions on Civil Engineering (A)

-  Volume 21 (2014)
-  Volume 20 (2013)
-  Volume 17 (2010)
-  Volume 16 (2009)
-  Volume 15 (2008)
-  Volume 14 (2007)
-  Volume 13 (2006)
-  Volume 12 (2005)
-  Volume 11 (2004)
-  Volume 10 (2003)
-  Volume 9 (2002)
-  Volume 8 (2001)
-  Volume 7 (2000)
-  Volume 6 (1999)
-  Volume 5 (1998)
-  Volume 4 (1997)
-  Volume 3 (1996)
-  Volume 2 (1995)
-  Volume 1 (1994)

[View Article](#)  PDF 2.58 M

Multi objective optimization of orthogonally stiffened cylindrical shells using optimality criteria method

Pages 717-727
Ghazaleh Eslami; Mohammad Z. Kabir

[View Article](#)  PDF 1.84 M

A seismic slope stability probabilistic model based on Bishop's method using analytical approach

Pages 728-741
A. Johari; S. Mousavi; A. Hooshmand nejad

[View Article](#)  PDF 3.36 M

[About Journal](#)

IF 2023: 1.4 2024-10-07

[Editorial Board](#)

[Submit Manuscript](#)

[Contact Us](#)

[Sitemap](#)

latest news and updates



Subscribe



This website uses cookies to ensure you get the best experience on our website.

Got it!



Sharif University of Technology
Scientia Iranica
Transactions A: Civil Engineering
 www.scientiairanica.com



Nonlinear finite element analysis of rectangular reinforced concrete slabs strengthened by fiber reinforced plastics

C. Lesmana^a and H.-T. Hu^{b,*}

a. *Department of Civil Engineering, Maranatha Christian University, Bandung 40164, Indonesia.*

b. *Department of Civil Engineering, National Cheng Kung University, Tainan 701, Taiwan, R.O.C.*

Received 9 January 2013; received in revised form 27 May 2014; accepted 5 August 2014

KEYWORDS

Finite Element
 Analysis (FEA);
 Reinforced concrete;
 Laminates;
 Slab;
 Numerical analysis;
 Strengthened.

Abstract. Strengthening reinforced concrete members by bonding fiber reinforced plastics on the tension face has become a viable alternative to address strength deficiency problems. This paper investigates rectangular composite slabs subjected to a distributed load using Abaqus finite element software. A parametric study, using appropriate constitutive models, is generated to stimulate the nonlinear material behavior of the reinforced concrete and FRP. The numerical analysis examines the behavior and maximum capacity of the composite slabs. The paper presents the finite element analysis results for concrete slabs strengthened with FRP material. The proposed fitted equation is applicable in the preliminary investigation for engineering applications.

© 2015 Sharif University of Technology. All rights reserved.

1. Introduction

Examination of the structural behavior of FRP-strengthened reinforced concrete structures, including beams, columns and slabs, has been carried out experimentally and theoretically. Laboratory testing is indeed necessary to obtain the actual behavior and failure modes of structures, but it is expensive and time consuming. Moreover, the existing structures are difficult to test to the point of ultimate failure. Since the scope of FRP utilization needs to be expanded, and efficient designs need to be provided, numerical studies are essential.

Finite Element (FE) analysis is an efficient and cost-effective numerical tool to model the structural behavior of RC members. It has been employed successfully to investigate the influences of a series

of parameters on the structural behavior of concrete structures [1]. The behavior model of the structures is necessary to obtain adequate results [4]. Most research has assumed FRP to be linear, but unidirectional fibrous composites exhibit severe nonlinearity in regard to their inplane shear stress-strain relations [5]. However, the degree of nonlinearity is not comparable to that observed with inplane shear, since deviation from linearity is observed with inplane transverse loading [5,6]. As a result, the nonlinear behavior of FRP should be modeled properly [7].

FRP laminates act as external reinforcements for concrete structures. Laminates that adhere to the tension face of structural elements provide additional flexural strength. There are a number of factors affecting the performance of the bonding mechanism between FRP and concrete, such as RC dimensions and mechanical properties, fiber orientation, fiber length, shape and composition of fibers, and the adhesion or bond between the fibers and RC [8]. Contribution of the stress strain relationship of FRP in composite elements, which are usually dramatically linear up

*. *Corresponding author. Tel.: 886-6-2757575;
 Fax: 886-6-2358542
 E-mail addresses: cindra@eng.maranatha.edu (C.
 Lesmana); hthu@mail.ncku.edu.tw (H.-T. Hu)*

to failure, without a discernible yield point, causes the non-plastic ultimate state of composite elements. Therefore, the key to designing a composite is to take advantage of the anisotropic nature of the FRP material and oriented fibers, and provide maximum stiffness with minimum materials [8].

To investigate the effect of nonlinear material behavior on composite slabs, analytical and mathematical models are adopted in this paper. The consequences of some factors, such as the aspect ratio of the slabs, FRP percentages and the orientation of the lamina angle on the ultimate load, are studied to observe the behavior and the maximum capacity of the composite slabs under specific circumstances. Furthermore, reliable verified factors are proposed for generating a preliminary investigation into the interactive design of general rectangular RC slabs strengthened with FRP.

2. Constitutive material laws

2.1. Concrete design model

Under multiaxial combinations of loading, the failure strengths of concrete are different from those observed under uniaxial conditions. However, the maximum strength envelope under multiple stress conditions seems to be largely independent of the load path [9]. In Figure 1, a Mohr-Coulomb type compression surface, together with a crack detection surface, is used to model the failure surface of concrete. When the principal stress components of concrete are in a biaxial compression zone, the response of the concrete is modeled by an elastic-plastic theory with an associated flow and an isotropic hardening rule. When the principal stress components of concrete are in either a biaxial tension zone or a biaxial tension-compression zone, cracking of the concrete is defined to occur via the crack

detection surface. Once the cracking of concrete takes place, the orientation of the crack is stored. Damaged elasticity is then used to model the existing crack [10].

When plastic deformation occurs, there should be a specific parameter to guide the expansion of the yield surface. A commonly used approach is to relate the multidimensional stress and strain conditions to a pair of quantities, namely, effective stress σ_c and effective strain ε_c , such that results obtained following different loading paths can all be correlated by means of the equivalent uniaxial stress-strain curve. For concrete nonlinear behavior, Saenz's stress-strain curve [11] is used. This relationship has been widely adopted as the uniaxial stress-strain curve for concrete, and it has the following form:

$$\sigma_c = \frac{E_c \varepsilon_c}{1 + (R + R_E - 2) \left(\frac{\varepsilon_c}{\varepsilon_o} \right) - (2R - 1) \left(\frac{\varepsilon_c}{\varepsilon_o} \right)^2 + R \left(\frac{\varepsilon_c}{\varepsilon_o} \right)^3}, \quad (1)$$

where:

$$R = \frac{R_E(R_\sigma - 1)}{(R_\varepsilon - 1)^2} - \frac{1}{R_\varepsilon},$$

$$R_E = \frac{E_c}{E_o},$$

$$E_o = \frac{f'_c}{\varepsilon_o},$$

and $R_\sigma = 4$, and $R_\varepsilon = 4$ are used [12]. In the analysis, Eq. (1) is taken as the equivalent uniaxial stress-strain curve for concrete. The value of ε_o is 0.003, as suggested by the ACI Committee 318 [13]. The initial modulus of the elasticity of concrete, E_c , can be calculated with reasonable accuracy from the empirical equation [13].

When cracking of concrete takes place, a smeared model is used to represent the discontinuous macro crack behavior. Tension stiffening, in which the cracked concrete of the RC element can still carry some tensile stress in the direction normal to the crack [14], is utilized by a simple descending line to model this tension stiffening phenomenon (Figure 2). The default

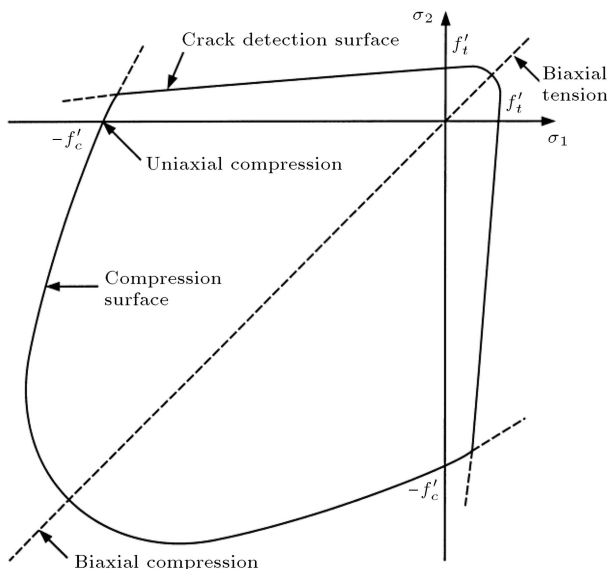


Figure 1. Concrete failure surface in plane stress.

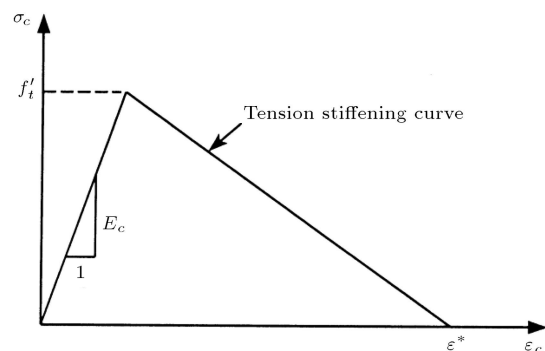


Figure 2. Tension stiffening model.

value of the strain, ε^* , at which the tension stiffening stress reduces to zero, is 0.001 [10].

During the post cracking stage, the cracked RC can still transfer shear forces through aggregate interlock or shear friction, which is termed shear retention. Assuming that the shear modulus of intact concrete is G_c , then the reduced shear modulus \hat{G} of cracked concrete can be expressed as:

$$\hat{G} = \mu G_c \quad \text{and} \quad \mu = (1 - \varepsilon/\varepsilon_{\max}),$$

where ε is the strain normal to the crack direction, and ε_{\max} is the strain at which the parameter μ reduces to zero. Numerous analytical results have demonstrated that the particular value chosen for μ (between 0 and 1) does not appear to be critical, but that values greater than zero are necessary to prevent numerical instabilities [14,15]. In Abaqus, ε_{\max} is usually assumed to be a very large value, i.e. $\mu = 1$ (full shear retention). In this investigation, the default values for tension stiffening parameter, $\varepsilon^* = 0.001$, and for shear retention parameter, $\mu = 1$, are used [10].

2.2. Steel reinforcement

The elastic modulus of the steel reinforcement is assumed to be $E_s = 200$ GPa. The elastic perfectly plastic is assumed to exemplify the stress-strain curve of the reinforcing bar. The steel reinforcement is treated as an equivalent uniaxial material smeared throughout the element section, and assumes a perfectly bond-slip model between concrete and steel. To properly model the constitutive behavior of the reinforcement, the cross sectional area, spacing, position and orientation of each layer of the steel bar within each element needs to be specified.

2.3. FRP reinforcement

For FRP (Figure 3), each lamina can be considered to be an orthotropic layer under a plane stress condition. It is well known that unidirectional fibrous composites exhibit severe nonlinearity in their inplane shear stress-strain relation. To model the nonlinear inplane shear

behavior, the nonlinear strain-stress relation for a composite lamina suggested by Hahn and Tsai [5] is adopted as follows:

$$\begin{Bmatrix} \varepsilon_1 \\ \varepsilon_2 \\ \gamma_{12} \end{Bmatrix} = \begin{bmatrix} \frac{1}{E_{11}} & -\frac{\nu_{21}}{E_{22}} & 0 \\ -\frac{\nu_{12}}{E_{11}} & \frac{1}{E_{22}} & 0 \\ 0 & 0 & \frac{1}{G_{12}} \end{bmatrix} \begin{Bmatrix} \sigma_1 \\ \sigma_2 \\ \tau_{12} \end{Bmatrix} + S_{6666} \tau_{12}^2 \begin{Bmatrix} 0 \\ 0 \\ \tau_{12} \end{Bmatrix}. \quad (2)$$

The FRP strain, ε_1 , ε_2 and γ_{12} , in longitudinal, transverse, and in-plane shear directions, respectively, can be calculated from the relationship between the stiffness matrix and the FRP stress, σ_1 , σ_2 and τ_{12} , in longitudinal, transverse and in-plane shear direction and the nonlinearity strain. In this model, only one constant, S_{6666} , is required to account for the inplane shear nonlinearity. The value of S_{6666} can be determined by a curve fit to various off-axis tension test data [5].

The incremental stress-strain relations for nonlinear orthotropic lamina can be given as follows:

$$\Delta\{\sigma'\} = [Q'_1]\Delta\{\varepsilon'\}, \quad (3)$$

$$\Delta\{\tau'_t\} = [Q'_2]\Delta\{\gamma'_t\}, \quad (4)$$

where:

$$\Delta\{\sigma'\} = \Delta\{\sigma_1, \sigma_2, \tau_{12}\}^T,$$

$$\Delta\{\tau'_t\} = \Delta\{\tau_{13}, \tau_{22}\}^T,$$

$$\Delta\{\varepsilon'\} = \Delta\{\varepsilon_1, \varepsilon_2, \gamma_{12}\}^T,$$

$$\Delta\{\gamma'_t\} = \Delta\{\gamma_{13}, \gamma_{22}\}^T,$$

and:

$$[Q'_1] = \begin{bmatrix} \frac{E_{11}}{1-\nu_{12}\nu_{21}} & \frac{\nu_{12}E_{22}}{1-\nu_{12}\nu_{21}} & 0 \\ \frac{\nu_{21}E_{11}}{1-\nu_{12}\nu_{21}} & \frac{E_{22}}{1-\nu_{12}\nu_{21}} & 0 \\ 0 & 0 & \frac{1}{\frac{1}{G_{12}} - 3S_{6666}\tau_{12}^2} \end{bmatrix}, \quad (5)$$

$$[Q'_2] = \begin{bmatrix} \alpha_1 G_{13} & 0 \\ 0 & \alpha_2 G_{23} \end{bmatrix}. \quad (6)$$

The terms α_1 and α_2 are the shear correction factors, and are taken to be 0.83 [16]. Furthermore, it is assumed that the transverse shear stresses always behave linearly and do not affect the nonlinear behavior of any inplane shear.

Among existing failure criteria, the Tsai-Wu criterion [17] has been extensively used in the literature

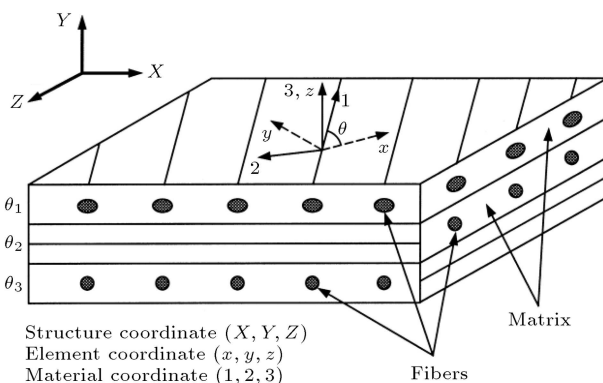


Figure 3. Material, element and structure coordinates of fiber reinforced plastics.

and is adopted in this analysis. Under plane stress conditions, this failure criterion has the following form:

$$F_1\sigma_1 + F_2\sigma_2 + F_{11}\sigma_1^2 + 2F_{12}\sigma_1\sigma_2 + F_{22}\sigma_2^2 + F_{66}\tau_{12}^2 = 1, \quad (7)$$

with:

$$F_1 = \frac{1}{\bar{X}} + \frac{1}{\bar{X}'}, \quad F_2 = \frac{1}{\bar{Y}} + \frac{1}{\bar{Y}'},$$

$$F_{11} = \frac{-1}{\bar{X}\bar{X}'}, \quad F_{22} = \frac{-1}{\bar{Y}\bar{Y}'}, \quad F_{66} = \frac{1}{\bar{S}^2}.$$

The \bar{X} , \bar{Y} and \bar{X}' , \bar{Y}' are the lamina longitudinal and transverse strengths in tension and compression, respectively, and \bar{S} is the shear strength of the lamina. Although it is difficult to determine the stress interaction term, F_{12} , in Eq. (7), it has been suggested that F_{12} can be set equal to zero for practical engineering applications [18]. Therefore, $F_{12} = 0$ is used in this investigation.

During the numerical calculation, incremental loading is applied to composite slabs until failures in one or more of the individual plies are indicated according to Eq. (7). Since the Tsai-Wu criterion does not distinguish failure modes, the following two rules are used to determine whether the ply failure is caused by debonding failure or FRP rupture [19]:

1. If a ply fails, but the stress in the fiber direction remains less than the uniaxial strength of the lamina in the fiber direction, i.e. $\bar{X}' < \sigma_1 < \bar{X}$, the ply failure is assumed to be resin induced. As a result, the laminate loses its capability to support transverse and shear stresses, but remains able to carry longitudinal stress. In this case, the constitutive matrix of the lamina becomes:

$$[Q'_1] = \begin{bmatrix} E_{11} & 0 & 0 \\ 0 & 0 & 0 \\ 0 & 0 & 0 \end{bmatrix}. \quad (8)$$

2. If a ply fails with σ_1 exceeding the uniaxial strength of the lamina, the ply failure is caused by fiber breakage, and a total ply rupture is assumed. In this case, the constitutive matrix of the lamina becomes:

$$[Q'_1] = \begin{bmatrix} 0 & 0 & 0 \\ 0 & 0 & 0 \\ 0 & 0 & 0 \end{bmatrix}. \quad (9)$$

During FE analysis, the constitutive matrix of composite materials at the integration points of shell elements must be calculated before the stiffness matrices are assembled from the element level to the structural

level. For composite materials, the incremental constitutive equations of a lamina in the element coordinates (x, y, z) can be written as:

$$\Delta\{\sigma\} = [Q_1]\Delta\{\varepsilon\}, \quad (10)$$

$$\Delta\{\tau_t\} = [Q_2]\Delta\{\gamma_t\}, \quad (11)$$

where:

$$\Delta\{\sigma\} = \Delta\{\sigma_X, \sigma_Y, \sigma_{XY}\}^T,$$

$$\Delta\{\tau\} = \Delta\{\tau_{XZ}, \tau_{YZ}\}^T,$$

$$\Delta\{\varepsilon\} = \Delta\{\varepsilon_X, \varepsilon_Y, \varepsilon_{XY}\}^T,$$

$$\Delta\{\gamma\} = \Delta\{\gamma_{XZ}, \gamma_{YZ}\}^T,$$

and:

$$[Q_1] = [T_1]^T [Q'_1] [T_1], \quad (12)$$

$$[Q_2] = [T_2]^T [Q'_2] [T_2], \quad (13)$$

$$[T_1] =$$

$$\begin{bmatrix} \cos^2 \theta & \sin^2 \theta & \sin \theta \cos \theta \\ \sin^2 \theta & \cos^2 \theta & -\sin \theta \cos \theta \\ -2 \sin \theta \cos \theta & 2 \sin \theta \cos \theta & \cos^2 \theta - \sin^2 \theta \end{bmatrix}, \quad (14)$$

$$[T_2] = \begin{bmatrix} \cos \theta & \sin \theta \\ -\sin \theta & \cos \theta \end{bmatrix}. \quad (15)$$

The θ is measured counterclockwise from the element local x axis to the material 1-axis (Figure 5). Let $\Delta\{\varepsilon_0\} = \Delta\{\varepsilon_{X0}, \varepsilon_{Y0}, \varepsilon_{XY0}\}^T$ be the incremental in-plane strains at the mid-surface of the shell section and $\Delta\{\kappa\} = \Delta\{\kappa_X, \kappa_Y, \kappa_{XY}\}^T$ be the incremental curvatures. The incremental inplane strains at distance z from the mid-surface of the shell section become:

$$\Delta\{\varepsilon\} = \Delta\{\varepsilon_0\} + z\Delta\{\kappa\}. \quad (16)$$

Let h be the total thickness of the composite shell section. The incremental stress resultants, $\Delta\{N\} = \Delta\{N_X, N_Y, N_{XY}\}^T$, $\Delta\{M\} = \Delta\{M_X, M_Y, M_{XY}\}^T$, and $\Delta\{V\} = \Delta\{V_X, V_Y\}^T$, can be defined as:

$$\begin{Bmatrix} \Delta\{N\} \\ \Delta\{M\} \\ \Delta\{V\} \end{Bmatrix} = \int_{-h/2}^{h/2} \begin{Bmatrix} \Delta\{\sigma\} \\ z\Delta\{\sigma\} \\ \Delta\{\tau_t\} \end{Bmatrix} dz. \quad (17)$$

Substituting Eqs. (10), (11) and (12) into the above expression, one can obtain the stiffness matrix for the

fiber composite laminate shell at the integration point as:

$$\begin{Bmatrix} \Delta\{N\} \\ \Delta\{M\} \\ \Delta\{V\} \end{Bmatrix} = \int_{-h/2}^{h/2} \begin{bmatrix} [Q_1] & z[Q_1] & [0] \\ z[Q_1] & z^2[Q_1] & [0] \\ [0]^T & [0]^T & [Q_2] \end{bmatrix} \begin{Bmatrix} \Delta\{\varepsilon_0\} \\ \Delta\{\kappa\} \\ \Delta\{\gamma_t\} \end{Bmatrix} dz, \quad (18)$$

where $[0]$ is a 3 by 2 null matrix. After Eq. (18) is developed in the element curvilinear coordinate (x, y, z) , it is automatically transformed into the global coordinate (X, Y, Z) by Abaqus to proceed with the assembly of the system. This transformation procedure involves element geometry, shape functions and a Jacobian matrix, which are specified in the Abaqus Theory Manual [10].

3. Numerical models

A large number of parameters were investigated to observe the behavior of the composite rectangular slabs. The slab models refer to experimental investigation by Mosallam and Mosalam [1]. The models, as illustrated in Figure 4, were subjected to uniform static pressure. The top surface was subjected to tensile stress, since the pressure was applied to the bottom surface of the slab. An equal spacing in the two orthogonal directions, #3@305 mm, was used for tension reinforcement

with grade 60. The yielding stress (f_y) was 413.7 MPa, and the compressive strength of the concrete (f'_c) was 32.87 MPa. Simply supported RC slab models were further generated with seven length aspect ratio models. The aspect ratio (a/b) is the length ratio that puts the length in the X and Y directions in contrast. The two types of designed slabs discussed herein were one-way slabs (i.e. $a/b = 2.5$, $a/b = 3$, $a/b = 3.5$ and $a/b = 4$) and two-way slabs ($a/b = 1$, $a/b = 1.5$, and $a/b = 2$).

The constitutive models from Section 2 were implemented into Abaqus to conduct failure analysis and to obtain the possible maximum ultimate load. Reliable constitutive models applicable to steel reinforcing bars and concrete are available in the Abaqus material library. For the FRP model, Abaqus has inbuilt failure criteria, such as Tsai-Wu, that has been used in much research [20-22]. However, these failure criteria only include the linear behavior of FRP. Therefore, FORTRAN language was used as a subroutine, UMAT, in Abaqus, to code nonlinear constitutive equations for including a nonlinear material library to model FRP. All the validity of the material models for steel, FRP and RC have been verified individually by testing against experimental data [4,10] and were not duplicated here. For rectangular RC slabs with and without FRP, the slabs have been verified against experimental data [4], and for square RC slabs with and without FRP, verification and numerical studies have also been performed [23] and were not duplicated here.

Since slabs have two planes of symmetry, only a 1/4 portion of the slab was analyzed, and symmetric boundary conditions were placed along the two symmetric planes. The RC rectangular slabs and FRP were modeled by eight-node quadrilateral shell elements with six degrees of freedom per node in a reduced integration rule. The mesh schemes for each case can be seen in Table 1. It can be seen that the FRPs are adhered from the center to the edge. Effects associated with the rebar/concrete interface, such as bond slip and dowel action, are modeled approximately by introducing some “tension stiffening” into the concrete cracking model to simulate load transfer across cracks through the rebar. Contribution of the adhesive layer to flexural capacity was neglected, and thus, it is assumed that there is perfect bonding between the FRP and the slab. This ‘no slip’ assumption has also been used by many investigators [24-26]. A very important aspect of bonded behavior is that there exists an effective bond length, beyond which an extension of the bond length cannot increase the bond strength, as well as the ultimate load, of the strengthened concrete structure. As long as the criterion for the effective bond length has been fulfilled, it is quite justifiable to use the perfect bonding assumption. An

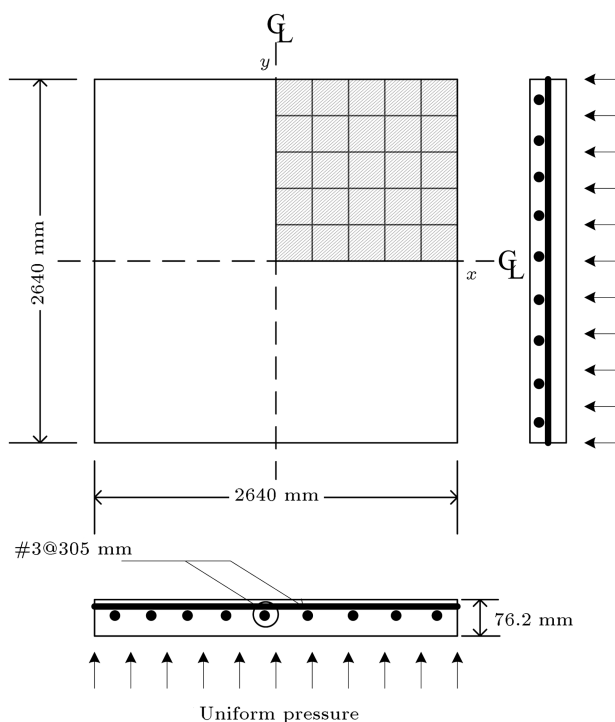


Figure 4. Detail of Mosallam-Mosalam specimens for reinforced concrete slab.

Table 1. Dimension of numerical reinforced concrete slab strengthened by FRP.

Model	Aspect ratio	Dimension		Number of elements ($n_x \times n_y$)					
		Lx (mm)	Ly (mm)	RC slab	Adhered FRP under specific ratios				
					4%	16%	36%	64%	100%
Type 2	$a/b = 1$	2640	2640	5×5	1×1	2×2	3×3	4×4	5×5
	$a/b = 1.5$	3960	2640	10×5	2×1	4×2	6×3	8×4	10×5
	$a/b = 2$	5280	2640	10×5	2×1	4×2	6×3	8×4	10×5
Type 1	$a/b = 2.5$	6600	2640	15×5	3×1	6×2	9×3	12×4	15×5
	$a/b = 3$	7920	2640	15×5	3×1	6×2	9×3	12×4	15×5
	$a/b = 3.5$	9240	2640	20×5	4×1	8×2	12×3	16×4	20×5
	$a/b = 4$	10560	2640	20×5	4×1	8×2	12×3	16×4	20×5

incremental-iterative Riks method [10] with automated load increment was used to solve the nonlinear finite element equations and to model the nonlinear structural behavior effectively. This method is necessary to obtain nonlinear static equilibrium solutions for unstable problems.

The FRP was adhered to the top side using a 0.58 mm thickness for each layer. The material properties of carbon FRP were adopted from the experimental specimens of Mosallam and Mosalam [1]. The tensile strength (X_{ut}) was 1208.7 MPa and the elastic modulus (E_{11}) was 100.75 GPa [1]. The following parameters were assumed to take the Tsai-Wu criterion into account:

$$E_{22} = 1 \text{ GPa}, \quad G_{12} = 1 \text{ GPa},$$

$$X_{uc} = -12 \text{ MPa}, \quad Y_{ut} = 12 \text{ MPa},$$

$$Y_{uc} = -12 \text{ MPa}, \quad S = 12 \text{ MPa},$$

$$S_{6666} = 0, \quad v_{12} = 0.3.$$

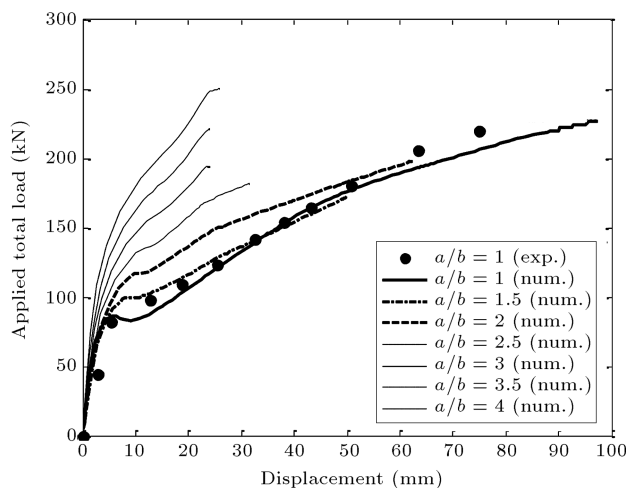
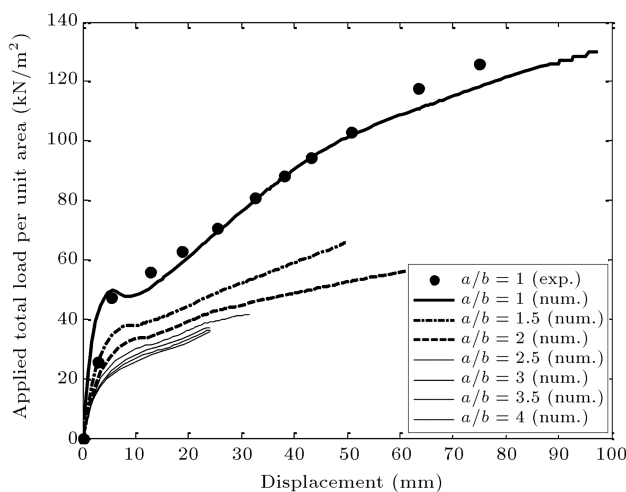
It is necessary to point out that a parameter of ε_{utf} , the ultimate strain of FRP in the fiber direction, was used. The value of ε_{utf} was limited to 0.008 [27]. To study the behavior of FRP in strengthened RC slabs, five cases of FRP ratio: 4%, 16%, 36%, 64%, and 100%, were measured. The FRP ratio was calculated as the ratio between the surface area of the slab, that was adhered using FRP, and the total area of the slab. To take advantage of the FRP material, a numerical analysis was conducted to simulate five combinations of angle laminates within two layers of FRP. The combinations were $[0/0]_n$, $[15, -15]_n$, $[30, -30]_n$, $[45/-45]_n$, and $[90/0]_n$ in which the fiber angle of the lamina was measured counterclockwise from the X-axis to the Y-axis and in which n was the number of layers; in this case, either one or two layers.

4. Parametric studies

4.1. Effect of aspect ratios on the maximum applied load of pure reinforced concrete slabs

Totally, seven models are discussed to represent two types of RC slab behavior: one-way, in which the slabs are designed to transfer their loads to only two opposite supports, and two-way, in which the slabs are designed to transfer their loads to all four sides. Type 1 is made up of three models of slabs with aspect ratios greater than two (one-way), and type 2 is made up of four models of slabs with aspect ratios less than, or equal to, two (two-way). The purposes are to evaluate the capacity of slabs with different aspect ratios and to observe the behavior of each different slab case. The results for the pure RC slabs become the baseline for the strengthening cases.

Figure 5 shows the curves for the applied total load and displacement at the center for pure RC slabs. A very good correlation can be observed between the numerical result ($a/b = 1$) and the experimental results of Mosallam and Mosalam. These good correlations between numerical predictions and experimental results demonstrate the validity of the nonlinear constitutive material models and the perfect bonding assumption between FRP and the slab. Contrasting the numerical curve for $a/b = 1$ and the experimental results, the numerical results can represent the stiffness of a real structure. Although the simulation cannot approach maximum displacement, the small percentage of standard error of 0.23% can be obtained for the ultimate load. In one-way slabs, Figure 5(a) for $a/b > 2$, the ultimate load and the stiffness increase as the aspect ratio becomes higher, while the stiffness of two-way slabs is relatively similar for different results of ultimate loads. Figure 5(b) shows that two-way slabs can resist higher load per unit area (P/A) if compared to one-way slabs. For one-way slabs, as the aspect ratio

(a) Applied total load (P) vs. displacement(b) Applied total load per unit area (P/A) vs. displacement**Figure 5.** Load and mid-span displacement curves of RC slabs in different aspect ratios.

becomes higher, the resisted load becomes lower. From all different a/b , the square slab ($a/b = 1$) exhibited the best performance, which had the highest ductility and the highest ultimate load.

4.2. Effect of fiber reinforced concrete percentages on strengthening composite slabs

In this study, the FRP shape remains rectangular for all aspect ratios, while the length is variable. The purposes are to evaluate whether FRP can strengthen the slabs under consideration and to examine whether adding more FRP can influence the ultimate load of the slabs. The applied total load and displacement at the center of the slab were plotted into curves to observe the effect of FRP in regard to strengthening the composite slabs. The plots illustrate the relationship using various cases of FRP ratios for different aspect ratios in $[90/0]_2$ combinations.

A higher FRP ratio indicates more reinforcement on the composite. Figure 6 demonstrates that increasing the FRP ratio results in a higher ultimate load. Taking $a/b = 1.5$ as an example, the maximum total loads increase to 189 kN, 225 kN, 300 kN, 442 kN, and 521 kN for FRP ratios of 4%, 16%, 36%, 64%, and 100%, respectively. In this case, 4% FRP can higher the total applied load into 1.1x from the slab without FRP, where 100% FRP can higher it into 3.03x. Such different increments can be obtained as the %FRP is increased. For load per unit area ($a/b = 1.5$), P/A increases to 72 kN/m², 86 kN/m², 115 kN/m², 169 kN/m², and 199 kN/m² for FRP ratios of 4%, 16%, 36%, 64%, and 100%, respectively. If P/A results for each different a/b are compared, Figure 6 shows that, as a/b becomes higher, the P/A result becomes lower. For example, the two-way slabs that are strengthened with 100% FRP can resist P/A as 328 kN/m² for $a/b = 1$, 199 kN/m² for $a/b = 1.5$, and 189 kN/m² for $a/b = 2$. Similar results can be observed from one-way slabs. The P/A results for the slabs strengthened with 4% FRP are 47 kN/m² for $a/b = 2.5$, 44 kN/m² for $a/b = 3$, 41 kN/m² for $a/b = 3.5$, and 39 kN/m² for $a/b = 4$. As FRP ratios increase, the ultimate loads increase gradually for a/b less than 2, and have significant increments for a/b greater than 2. Type 1 slabs with greater FRP ratios produce more significant ultimate loads, as compared to type 2 slabs.

Higher FRP ratios provide higher stiffness, but this is sometimes followed by lower ductility, which affects the brittleness of composite slabs. This indication is shown in Figure 6 for $a/b = 1$, $a/b = 1.5$, and $a/b = 2$ where, compared with pure RC, most of the composite slabs have higher stiffness and higher ultimate load but lower ductility. On the other hand, higher stiffness and higher ductility can be found for a/b greater than two. The composition of the FRP should be designed carefully to prevent member failure accordingly. Nevertheless, engineers need to consider how to provide higher ultimate load with a minimum amount of FRP material.

4.3. Effect of the fiber angle in composite slabs

The performance of a composite may be affected by fiber orientation. The purposes of this analysis are to examine whether the angle direction can increase the load increment ratio, and affect the nonlinearity of FRP behavior in composite slabs. Considering Figure 7, the nonlinear shear of the FRP does not appear to have significant results. For example, in $a/b = 1$, the curves for $[15/-15]_2$, $[30/-30]_2$, and $[45/-45]_2$ are roughly parallel with $[0]_4$ and $[90/0]_2$, which have no nonlinear shear effects. The nonlinear effect is barely shown in all aspect ratios. Owing to the small failure shear strain of the composite slabs, the material nonlinearity of FRP,

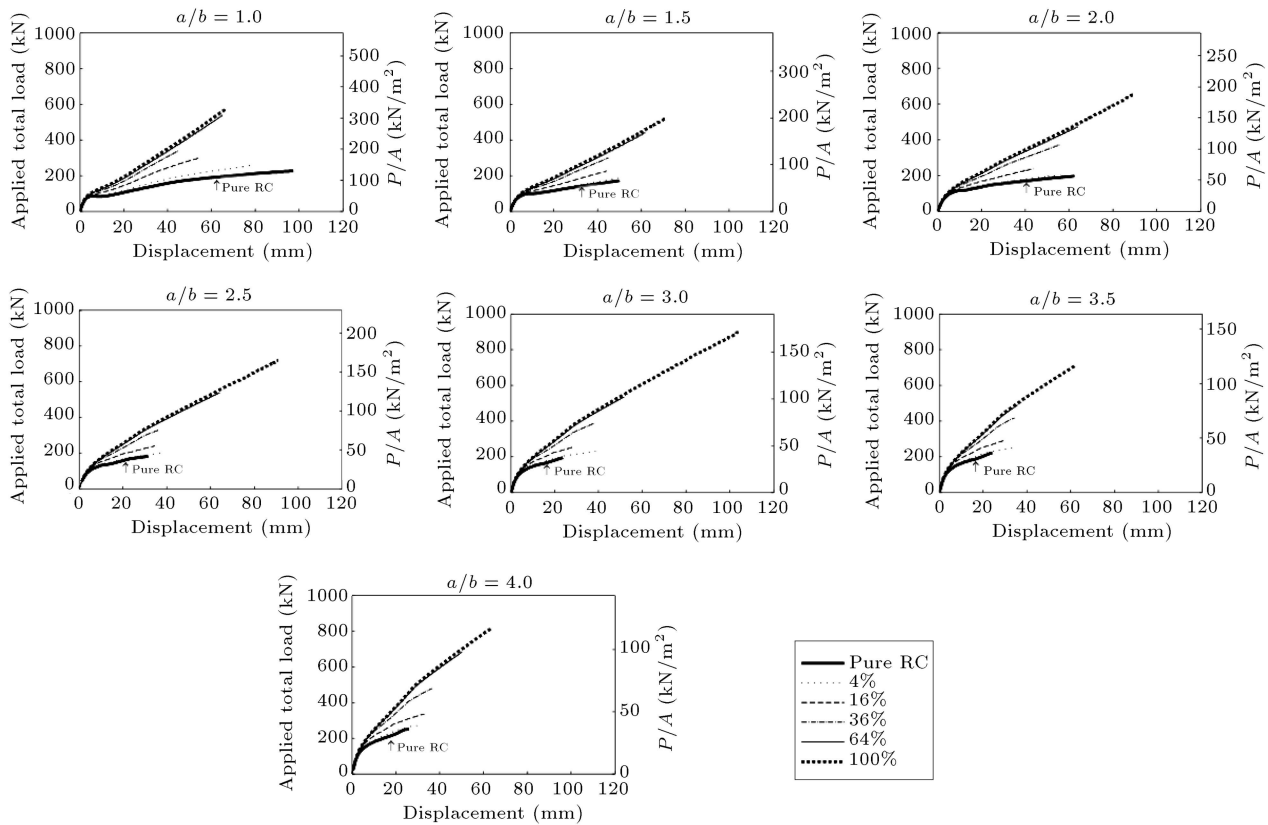


Figure 6. Load and mid-span displacement curves of the strengthened slabs in different aspect ratios for various FRP ratios with angle of lamina $[90/0]_2$.

in regard to the inplane shear stress-strain relationship of the ply, does not have too much influence on the behavior of the composite square slabs.

For type 1 (Figure 7 for $a/b > 2$), only the combination of ply $[90/0]_2$ obtains significant results, high ultimate load, high stiffness and high ductility. Other ply combinations only strengthened the slabs, without optimal results. Figure 7 for $a/b \leq 2$, two-way slabs, presents different ultimate loads for each combinations of ply orientation. The best combinations for stiffness and ultimate load differ for each case of aspect ratios. For example, the best combination for $a/b = 1$, $a/b = 1.5$, and $a/b = 2$, for the highest stiffness and highest load, are shown to be $[45/-45]_2$, $[45/-45]_2$, and $[90/0]_2$, respectively. Since other combinations are also relevant, with regard to application in two-way composite slabs, the best combination of ply orientation is essential to optimize the FRP application.

One-way slabs demonstrate structural strength in the shortest direction since the loads are resisted by the slab in one direction only. As a result, only a fiber orientation parallel to the distributed load of 90° is observed to have significant results. On the contrary, the loads resisted by all four sides in two-way slabs generate different optimum combinations of fiber orientation.

4.4. Effect of number of layers in composite slabs

In this section, two-layer FRP laminates are compared to one layer of FRP. The results are discussed with regard to observing the effect of the number of layers and thicknesses, on the increment ratio. Figure 7 demonstrates the results for the composite slabs with different numbers of FRP layers. The results are generated from fiber orientation of $[0/90]$ for one layer FRP and $[90/0]_2$ for two-layer FRP. Adding more layers of FRP generates higher ultimate load. A significant increment appears in one-way slabs with higher FRP ratios. As a/b becomes lower, the significant effect of adding layers and fiber orientation can be disregarded.

The effect of FRP layer and %FRP combined into FRP reinforcement ratio (ρ_f) can be derived as:

$$\rho_f = \frac{A_f}{b.d}, \quad (19)$$

with the total area of FRP (A_f) calculated from the number of FRP layers (n_f), width of FRP (b_f), and thickness of each FRP layer (t_f) as $A_f = n_f b_f t_f$. The ρ_f for 4% FRP, 16% FRP, 36% FRP, 64% FRP, and 100% FRP are 0.0018, 0.0037, 0.0055, 0.0073, and 0.0091 (the composite slabs with one FRP layer), respectively, and 0.0037, 0.0073, 0.0110, 0.0146, and 0.0183 (the composite slabs with one FRP layer),

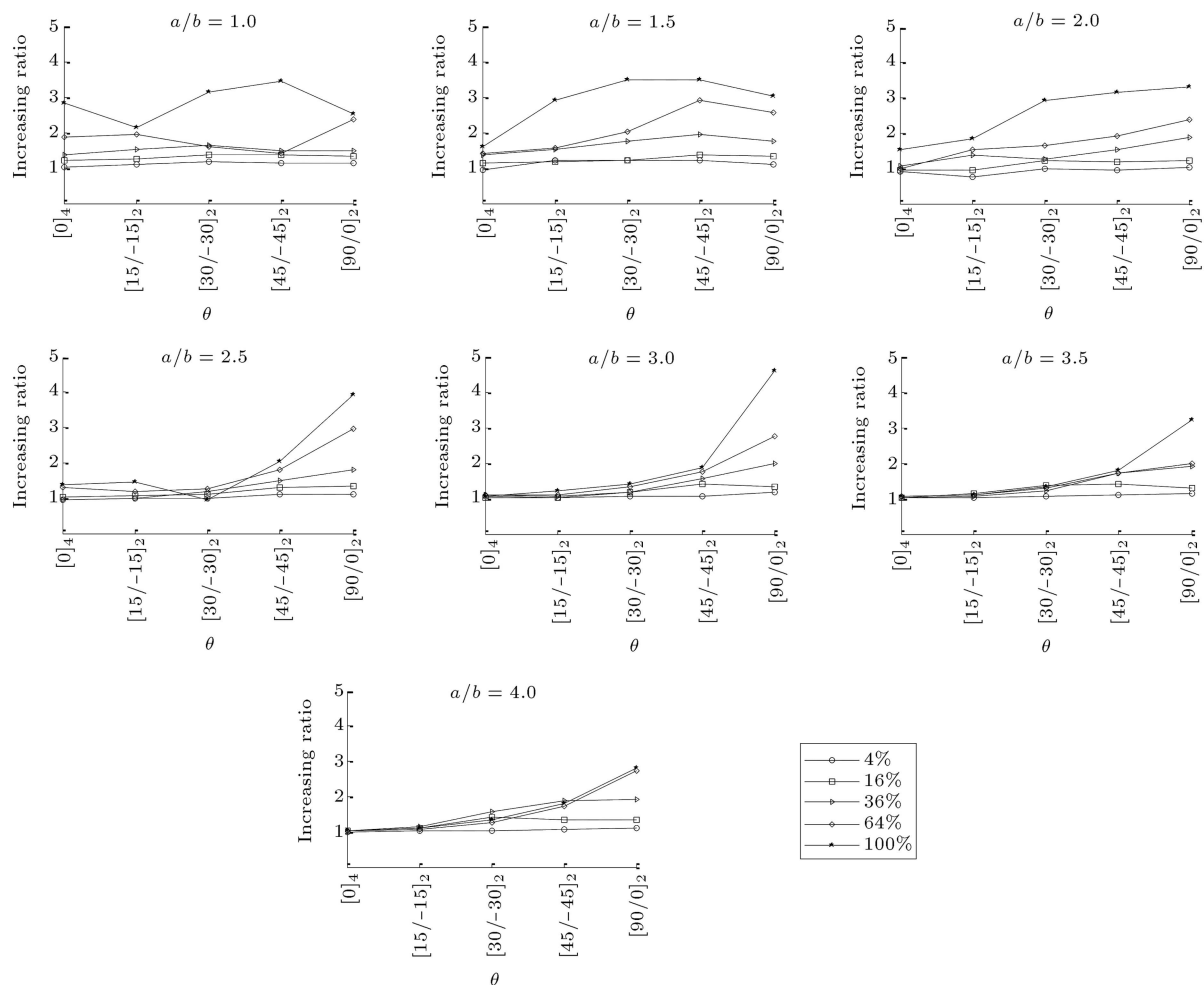


Figure 7. Comparison of the increasing ultimate load ratio for varied FRP ratio in different fiber laminates.

respectively. Figure 8 presents the results for 16% FRP $[90/0]$, which are similar to the results for 4% FRP $[90/0]_2$, and the results for 64% FRP $[90/0]$ are similar to the results for 16% FRP $[90/0]_2$. Adhering further FRP layers into RC slabs is equivalent to adding more reinforcement to the slabs. They can increase the ultimate load of the composite until a certain limit, after which, adhering more FRP will not cause significant results.

5. Results and discussion

To indicate a “tough” composite, the energy stored at failure is presented by calculating the area under the load and displacement curves. Excellent composite slabs are those having an energy value that is as high as possible. Figure 9 demonstrates that the energy stored at failure gradually increases as FRP ratio increases. To develop high-quality composite, the important thing is not only to obtain composites with a higher degree of stiffness, but also to determine a method by which a composite can be utilized with a minimum amount of material. Engineers should

be aware that attaching more FRP will not create impressive stiffness, especially in the case of two-way slabs. Thus, determining how to design the right combination of ply orientation with an appropriate FRP ratio is more important.

Most of the results (Figure 9 for $a/b > 2$) show that the energy stored at failure is occupied by fiber orientation $[90/0]_2$. The result in Figure 8 also shows that it is not recommended to attach ply other than $[90/0]_2$ for $a/b > 2$. Therefore, the higher FRP ratios in one-way slabs may not provide significant increases in the energy stored at failure without any proper combination of fiber orientation.

A higher FRP ratio creates higher strain energy. Figure 9 illustrates the strain energy results for each simulation case. Unexpected indications show that the composite slabs can have the same or lower strain energy than pure RC slabs. Especially, in the case of $a/b \leq 2$, “tough” composites were slabs with FRP ratios greater than 36% with proper ply combinations. For $a/b > 2$, the strain energy of composite slabs was shown to be broadly the same as, or greater than, pure RC. The results in $[90/0]_2$ orientation showed

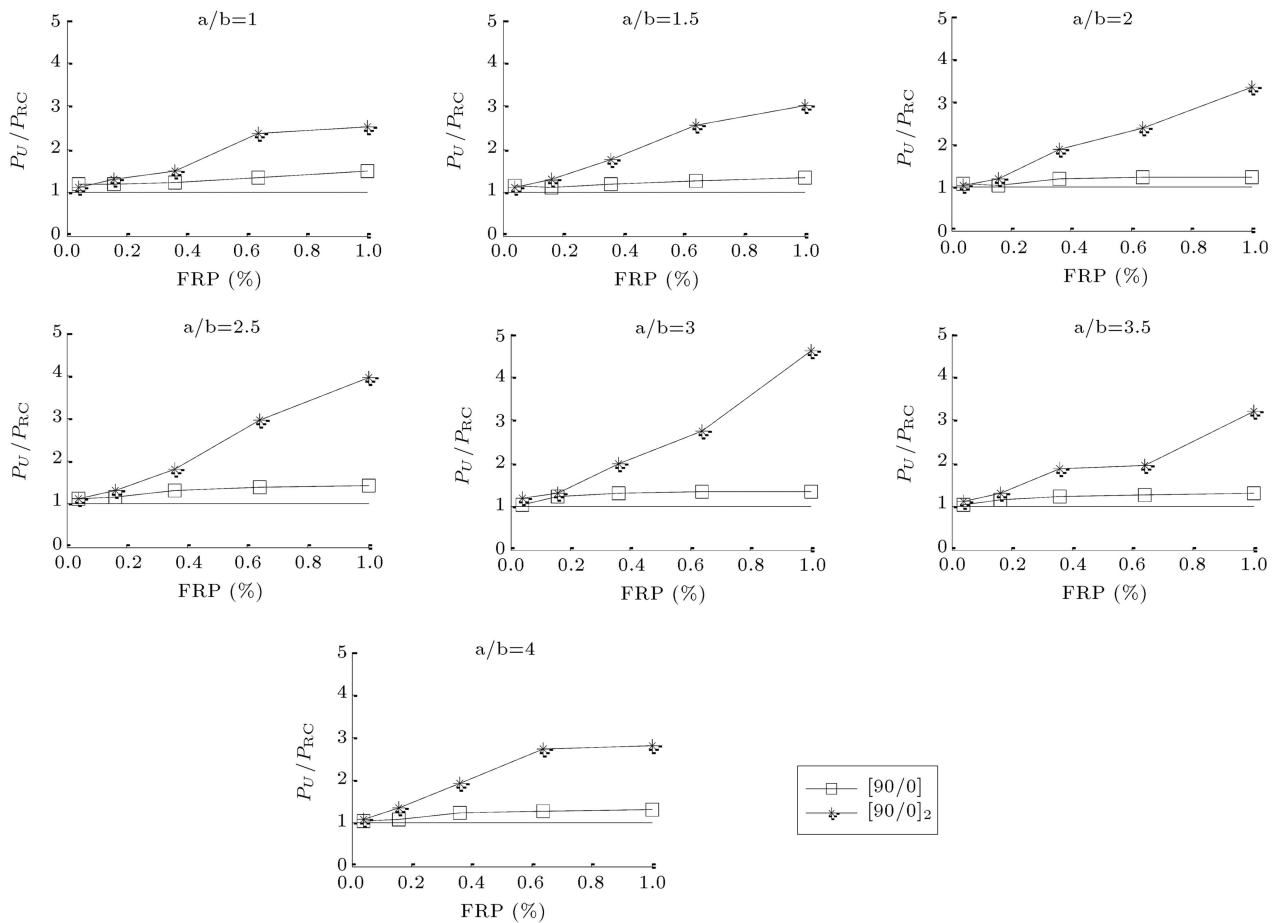


Figure 8. Comparison of the increasing ultimate load ratio for varied FRP ratio in different number of layers.

tremendously greater strain energy for an FRP ratio of more than 64%. Although other combinations of fiber orientation can result in higher stiffness, the best orientation, in regard to producing higher strain energy and resisting higher ultimate load, was found to be $[90/0]_2$.

Figure 10 shows efficiency of the composite slabs with different aspect ratios and fiber orientation. It demonstrates that higher FRP ratios have lower efficiency in return. In contrast, most of the “tough” composite slabs were shown to have lower efficiency. In general, FRP ratios more than 16% are recommended. The slabs that adhered more than 16% FRP had high strain energy and acceptable efficiency. It should be noted that in the case of one-way slabs, since attaching more than 16% FRP in $[90/0]_2$ orientation provides roughly the same efficiency, the design consideration must depend on targeted ultimate loads. For two-way slabs, the best combination of ply orientation and targeted ultimate loads are essential in the design.

Finally, the numerical results were plotted to develop an innovative curve for investigation of the composite slabs. MATLAB [28] was used as a tool. A curve fitting toolbox provides an application and functions for fitting curves and surfaces to data that can

perform data analysis, and preprocess and post-process data. A three-dimensional curve was associated with the FRP reinforcement ratio (ρ_f) in the x direction, aspect ratio (a/b) in the y direction, and increment ratio (P_u/P_{RC}) in the z direction. The R-square for the fitting curve was 91.25%, which indicates that the fitting can predict the estimated increment ratio closely fit to the numerical data. Figure 11 presents the curve fitting to optimize the recommendation for strengthening the RC slabs by carbon FRP. The fitting begins with the equation for two-way slabs, $1 \leq a/b \leq 2$, as:

$$P_u/P_{RC} = 1.6 - 100 \times (\rho_f) - 0.3 \times (a/b) + 7454 \times (\rho_f)^2 + 45 \times (\rho_f) \times (a/b). \quad (20)$$

For different values of a/b in the range of $2 < a/b \leq 4$, the following expressions are used.

$$P_u/P_{RC} = 1.075 - 26 \times (\rho_f) + 8215 \times (\rho_f)^2 \quad \text{for } a/b = 2.5, \quad (21)$$

$$P_u/P_{RC} = 1.150 - 42 \times (\rho_f) + 8977 \times (\rho_f)^2 \quad \text{for } a/b = 3, \quad (22)$$

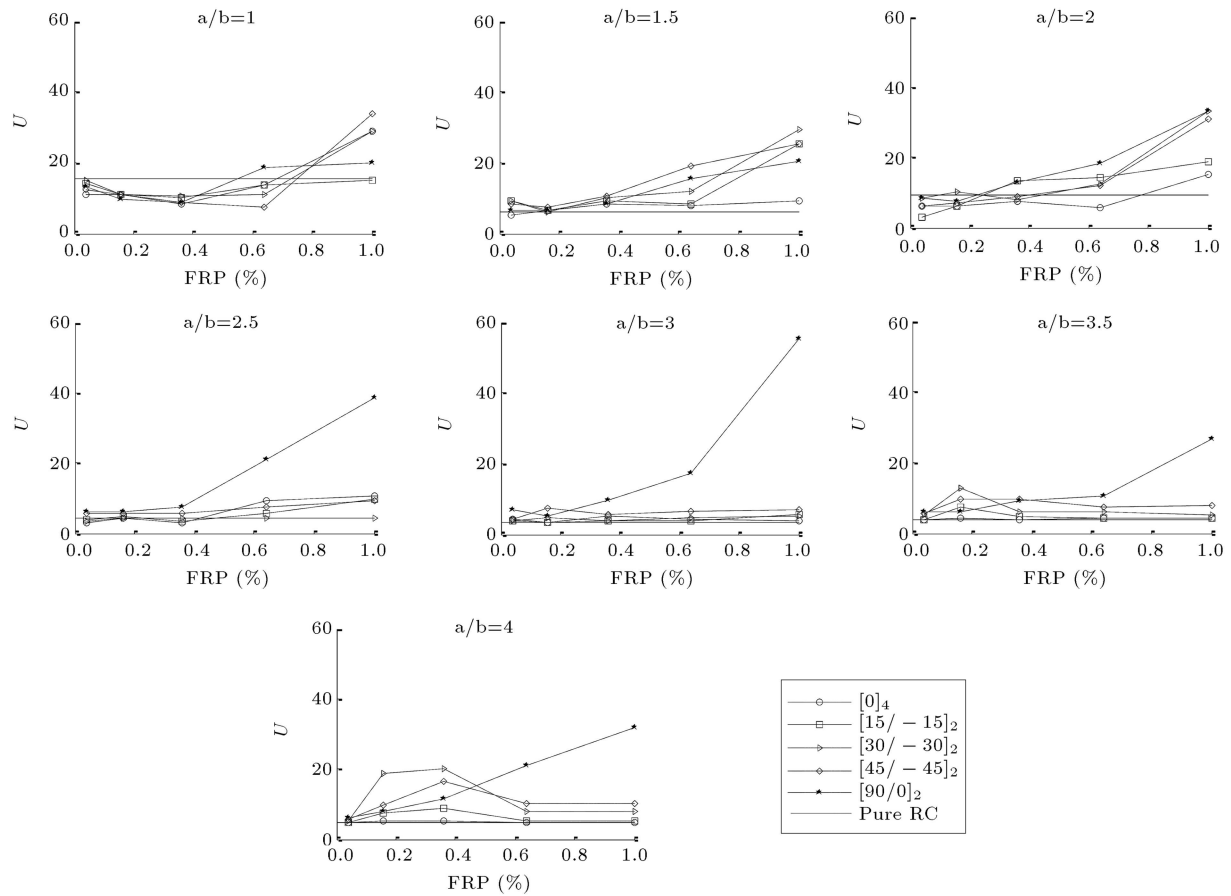


Figure 9. Comparison of the energy stored at failure of different aspect ratios for varied FRP ratio in different fiber laminates.

$$P_u/P_{RC} = 1.225 - 58 \times (\rho_f) + 9739 \times (\rho_f)^2$$

for $a/b = 3.5$, (23)

$$P_u/P_{RC} = 1.300 - 74 \times (\rho_f) + 10500 \times (\rho_f)^2$$

for $a/b = 4$. (24)

Figure 12(a) demonstrates the relationship between FRP reinforcement ratios and increasing ratios for various a/b . An increasing ratio can be described as quadratic with a positive slope for which the increasing ratios will be higher if more FRPs are attached to the RC slabs. On the other hand, the relationships between a/b and P_u/P_{RC} are not always increased as a/b increases. It is shown in Figure 12(b) that the P_u/P_{RC} will have a negative slope for $1 \leq a/b \leq 2$ (two-way slab) and a positive slope $2 < a/b \leq 4$ (one-way slab) at lower FRP reinforcement ratios ($\rho_f < 0.0073$). On the contrary, as the ratios become higher, the trends are reversed, indicating a positive slope for one-way slabs and a negative slope for two-way slabs.

Eqs. (21) to (24) would be suitable for practical engineering. These empirical equations are limited to

the preliminary investigation for composite rectangular slabs ($1 \leq a/b \leq 4$) strengthened by two-layer carbon FRP with a ply orientation of $[90/0]_n$ in which n equals one or two. They can estimate either the increment of the ultimate load using FRP reinforcement ratio assessment or the minimum requirement of FRP reinforcement ratios to attain a certain increment of ultimate load for certain aspect ratios. Nevertheless, a detailed design should be performed before the composite slab is applied in engineering practices, and the best combination of fiber orientation needs to be found in two-way slabs in order to obtain optimum design.

6. Conclusions

In this paper, nonlinear finite element analyses for strengthening rectangular RC slabs by bonding FRP are performed. Based on the numerical results, the following conclusions may be drawn:

1. In the case of pure RC slabs, the square slab ($a/b = 1$) has the best performance in regard to ductility and ultimate load.
2. Adding further areas of FRP in composite slabs

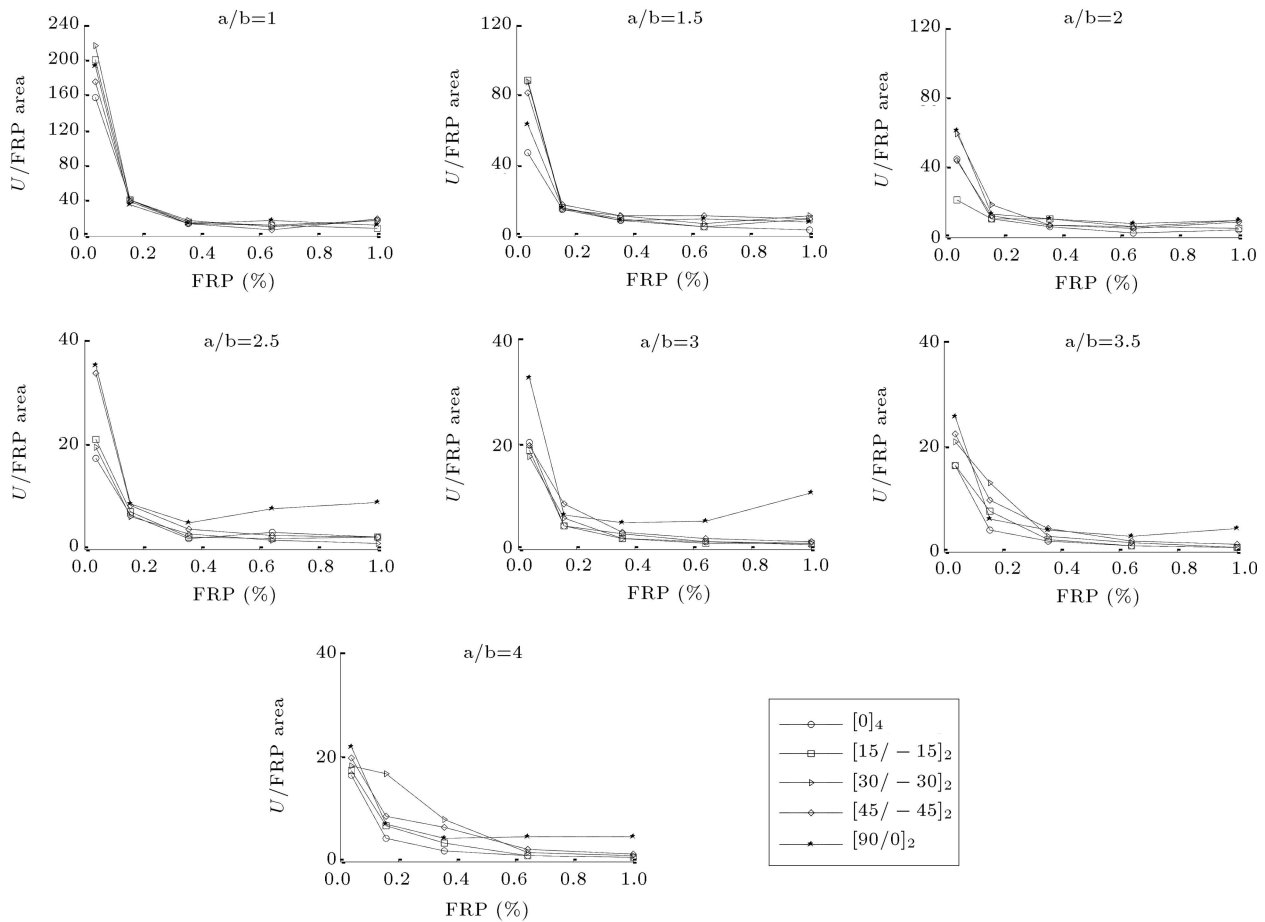


Figure 10. Comparison of the efficiency of different aspect ratios for varied FRP ratios in different fiber laminates.

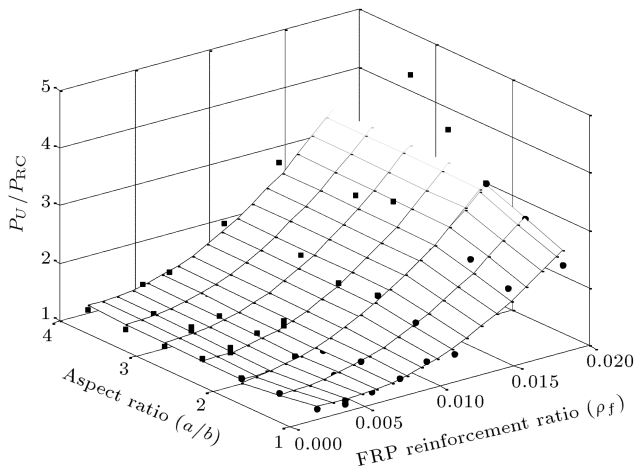


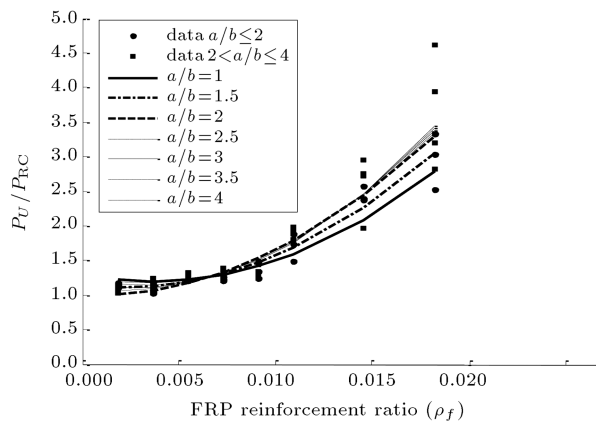
Figure 11. The summary results of strengthening of RC square slabs in different aspect ratios and FRP ratios.

offers higher stiffness, but may be followed by lower ductility. Compared with two-way slabs ($2 < a/b \leq 4$), attaching more FRPs in one-way RC slabs ($1 \leq a/b \leq 2$) produces better results for higher ultimate load, stiffness, and ductility.

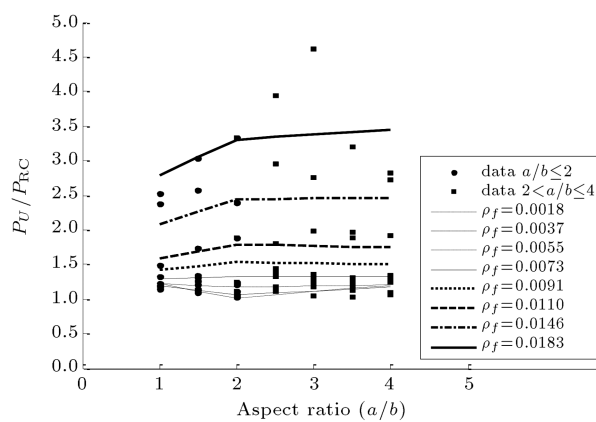
- Owing to the small failure shear strain of the composite slabs, the material nonlinearity of FRP

in an inplane shear stress-strain relation does not have a significant influence on the behavior of the composite square slabs.

- In one-way slabs ($1 \leq a/b \leq 2$), a fiber orientation normal to the longitudinal direction of the slab (90°) is recommended, since the load is resisted in one direction only. However, in two-way slabs ($2 < a/b < 4$), the loads are distributed in both directions, so the best combination of fiber orientation needs to be found.
- Adhering further FRP layers into composite slabs is equivalent to adding more reinforcement into the composites. The FRPs in the tensile surface can strengthen the composite slab until a certain limit after which adhering more FRP will not cause significant results in increasing the ultimate load.
- A “tough” composite has lower efficiency. The more FRP is adhered to the composite slabs, the more ultimate load can be obtained, but lower efficiency is a result. It is essential to design the right combination of fiber orientation in an appropriate FRP ratio.
- Generalizations in preliminary investigative approaches are generated for strengthening rectangu-



(a) FRP reinforcement ratio vs. increasing ratio



(b) Aspect ratio vs. increasing ratio

Figure 12. The relationship among increasing ratio (P_u/P_{RC}), aspect ratio (a/b) and FRP reinforcement ratio (ρ_f).

lar RC slabs ($1 \leq a/b \leq 4$) with two-layer carbon FRP. A detailed design should be analyzed carefully before FRP is applied in engineering practices. Due to simplicity, a perfect bond is assumed in this numerical modeling, however, in real structures, debonding might be a dominant failure mode and, so, should be formulated in further research.

References

- Mosallam, A.S. and Mosalam, K.M. "Strengthening of two-way concrete slabs with FRP composite laminates", *Construction and Building Materials*, **17**(1), pp. 43-54 (2003).
- Ascione, F., Berardi, V.P., Feo, L. and Giordano, A. "An experimental study on the long-term behavior of CFRP pultruded laminates suitable to concrete structures rehabilitation", *Composites Part B: Engineering*, **39**(7-8), pp. 1147-1150 (2008).
- Al-Zaid, R.Z., Al-Negheimish, A.I., Al-Saawani, M.A. and El-Sayed, A.K. "Analytical study on RC beams strengthened for flexure with externally bonded FRP reinforcement", *Composites Part B: Engineering*, **43**(2), pp. 129-141 (2012).
- Hu, H.-T., Lin, F.-M., Liu, H.-T., Huang, Y.-F. and Pan, T.-C. "Constitutive modeling of reinforced concrete and prestressed concrete structures strengthened by fiber-reinforced plastics", *Composite Structures*, **92**(7), pp. 1640-1650 (2010).
- Hahn, H.T. and Tsai, S.W. "Nonlinear elastic behavior of unidirectional composite laminae", *Journal of Composite Materials*, **7**(1), pp. 102-118 (1973).
- Jones, R.M. and Morgan, H.S. "Analysis of nonlinear stress-strain behavior of fiber-reinforced composite materials", *AIAA Journal*, **15**(12), pp. 1669-1676 (1977).
- Hu, H.-T. and Schnobrich, W.C. "Nonlinear finite element analysis of reinforced concrete plates and shells under monotonic loading", *Computers & Structures*, **38**(5-6), pp. 637-651 (1991).
- ACI Committee 440, State-of-the-Art Report on Fiber Reinforced Plastic (FRP) Reinforcement for Concrete Structures, American Concrete Institute, ACI 440R-96 (2002).
- Kupfer, H., Hilsdorf, H.K. and Rusch, H. "Behavior of concrete under biaxial stresses", *ACI Structural Journal*, **66**, pp. 656-666 (1969).
- Abaqus Inc., Abaqus Analysis User's Manuals and Example Problems Manuals, Version 6.13, Providence, Rhode Island (2013).
- Saenz, L. "Discussion of "Equation for the stress-strain curve of concrete" by Desayi P and Krishnan S", *ACI Structural Journal*, **61**(9), pp. 1229-1235 (1964).
- Hu, H.-T. and Schnobrich, W.C. "Constitutive modeling of concrete by using nonassociated plasticity", *Journal of Materials in Civil Engineering, ASCE*, **1**(4), pp. 199-216 (1989).
- ACI Committee 318, Building Code Requirements for Structural Concrete and Commentary (ACI 318-08), Detroit, Michigan (2011).
- ASCE Task Committee on Concrete and Masonry Structure, State of the Art Report on Finite Element Analysis of Reinforced Concrete, ASCE (1982).
- Hu, H.-T. and Schnobrich, W.C. "Nonlinear analysis of cracked reinforced concrete", *ACI Structural Journal*, **87**(2), pp. 199-207 (1990).
- Mindlin, R.D. "Influence of rotary inertia and shear on flexural motions of Isotropic, elastic plates", *ASME Journal of Applied Mechanics*, **18**, pp. 31-38 (1951).
- Tsai, S.W. and Wu, E.M. "A general theory of strength for anisotropic materials", *Journal of Composite Materials*, **5**(1), pp. 58-80 (1971).
- Narayanaswami, R. and Adelman, H.M. "Evaluation of the tensor polynomial and Hoffman strength theories for composite materials", *Journal of Composite Materials*, **11**(4), pp. 366-377 (1977).
- Rowlands, R.E. "Strength (failure) theories and their experimental correlation", *Failure Mechanics of Composites*, handbook of composites, **3**, New York: North-Holland, pp. 71-128 (1985).

20. Mahini, S.S., Hadigheh, S.A. and Maheri, M.R. "Seismic assessment of FRP-retrofitted RC frames using pushover analysis considering strain softening of concrete", In: Ye, L., Feng, P., Yue, Q., Eds., *Advances in FRP Composites in Civil Engineering*, Springer Berlin Heidelberg, pp. 841-844 (2011).
21. Hadigheh, S.A., Maheri, M.R. and Mahini, S.S. "Performance of weak-beam, strong-column RC frames strengthened at the joints by FRP", *Transactions of Civil Engineering*, **37**(C1), pp. 33-51 (2013).
22. Mostofinejad, D., Moshiri, N. and Mortazavi, N. "Effect of corner radius and aspect ratio on compressive behavior of rectangular concrete columns confined with CFRP", *Mater. Struct.*, pp. 1-16 (2013).
23. Lesmana, C., Hu, H.-T., Lin, F.-M. and Huang, N.-M. "Numerical analysis of square reinforced concrete plates strengthened by fiber-reinforced plastics with various patterns", *Composites Part B: Engineering*, **55**(0), pp. 247-262 (2013).
24. Fraldi, M., Nunziante, L., Carannante, F., Prota, A., Manfredi, G. and Cosenza, E. "On the prediction of the collapse load of circular concrete columns confined by FRP", *Engineering Structures*, **30**(11), pp. 3247-3264 (2008).
25. Mahini, S.S. and Ronagh, H.R. "Numerical modelling of FRP strengthened RC beam-column joints", *Structural Engineering and Mechanics*, **32**(5), pp. 649-665 (2009).
26. Teng, J., Chen, J., Smith, S. and Lam, L., *FRP Strengthened RC Structures*, John Wiley & Sons, Inc. (2002).
27. The Concrete Society Technical Report 55, *Design Guidance for Strengthening Concrete Structures Using Fibre Composite Materials*, Crowthorne, UK (2000).
28. The MathWorks, I., MATLAB - The Language of Technical Computing, Version 7.10, The MathWorks Inc., Natick, Massachusetts (2010).

Biographies

Cindrawaty Lesmana received her MS degree in Construction Engineering from the National Taiwan University of Science and Technology and a PhD degree in Civil Engineering from the National Cheng Kung University, Taiwan. Her research interests include structural analysis using FEM, reinforced concrete structures, structural assessment and earthquake mitigation.

Hsuan-Teh Hu received MS and PhD degrees in Civil Engineering from the University of Illinois at Urbana-Champaign, USA, in 1983 and 1988, respectively. He is currently Professor in the Department of Civil Engineering at the National Cheng Kung University, Taiwan. His research interests include plates and shells, fiber-reinforced plastic materials, reinforced concrete, and structural optimization.